Highlights of Spanish Astrophysics XII, Proceedings of the XVI Scientific Meeting of the Spanish Astronomical Society held on July 15 - 19, 2024, in Granada, Spain. M. Manteiga, F. González Galindo, A. Labiano Ortega, M. Martínez González, N. Rea, M. Romero Gómez, A. Ulla Miguel, G. Yepes, C. Rodríguez López, A. Gómez García and C. Dafonte (eds.), 2025

Injection of water vapor into the Martian upper atmosphere during the perihelion season observed with ExoMars-TGO/NOMAD

Brines, A.[1], Lopez-Valverde, M. A.[1], Funke, B.[1], Gonzalez-Galindo, F.[1], Aoki, S.[2,3], Villanueva, G.[4], Holmes, J.[5], Belyaev, D.[6], Liuzzi, G.[7], Thomas, I.[3], Erwin, J.[3], Grabowski, U.[8], Forget, F.[9], Lopez-Moreno, J. J.[1], Rodriguez-Gomez, J.[1], Sanz-Mesa, R. M.[1], Daerden, F.[3], Trompet, L.[3], Ristic, B.[3], Patel, M.[3], Bellucci, G.[10], and Vandaele, A. C.[3]

[1] Instituto de Astrofísica de Andalucía (IAA/CSIC), Spain
[2] Department of Complexity Science and Engineering, University of Tokyo, Japan
[3] Royal Belgian Institute for Space Aeronomy, Belgium
[4] NASA Goddard Space Flight Center, USA
[5] Open University, UK
[6] Space Research Institute, Moscow, Russia
[7] University of Basilicata, Italy
[8] Karlsruhe Institute of Technology, Karlsruhe, Germany
[9] Laboratoire de Météorologie Dynamique, IPSL, Paris, France
[10] Istituto di Astrosica e Planetologia, Italy

Abstract

We analyzed infrared spectra observed with the ExoMars-TGO/NOMAD instrument during the perihelion and Southern summer solstice season (L_S =240°-300°) spanning over three Martian Years, namely MY 34, 35 and 36. This is known to be the warmer and dustier season on Mars, playing a key role on the atmospheric escape of hydrogen to space. We present water vapor vertical profiles showing the detailed latitudinal distribution of H_2O at tangent altitudes from 10 to 120 km, revealing a strong vertical plume at 60°S - 50°S. This feature injects H_2O into the mesosphere, reaching abundances around 50 parts per million by volume (ppmv) at 100 km. We observed this event repeatedly in the three Martian years analyzed, although with inter-annual variations in both its magnitude and timing, possibly due to indirect effects of a global dust storm which occurred on MY 34. We suggest this event weakened the Southern Polar Vortex and may have allowed atmospheric dust to deposit over the Southern polar water ice reservoirs, leading to a reduced water vapor production rate during the perihelion of MY 34, and consequently, affecting the appearance and intensity of this plume that year. We estimated a projected hydrogen escape of 3.2×10^9 $cm^{-2}s^{-1}$ associated to these plumes, representing a 35% increase of our estimation outside the plumes, adding further evidence of the key role played by the perihelion season in the long term evolution of the planet's climate.

1 Introduction

The Mars we observe today is a dry and cold planet, although there are abundant evidences on the surface suggesting a warmer and wetter environment in the past [1]. Despite being a minor species in the current Martian atmosphere (∼0.03%), water vapor has a large variability throughout the year, resulting in a very complex hydrological cycle involving sublimation and condensation processes affected by dust and atmospheric transport [2].

Water is present (in vapor or ice phase) in most of the radiative and chemical processes driving the Martian climatology. However, until the last decade, the knowledge about the water vapor vertical distribution on Mars was limited, and the water cycle has been studied mainly with the analysis of column density abundances [2]. Recent Solar Occultation (SO) observations with the ExoMars Trace Gas Orbiter (TGO) allowed to explore the atmospheric vertical distribution in unprecedented detail, opening a new path towards a better understanding of the Martian climate. We present here a summary of the recent results from [3], devoted to characterize the water vapor in the Martian atmosphere with vertical profiles up to 120 km altitude. In Section 2 we present the NOMAD instrument and the data analysis methodology. In Section 3 we study the water vapor latitudinal distribution during 3 Martian Years (MYs 34, 35 and 36). Here we analyze 1065 NOMAD SO observations during specific solar longitude (L_S) periods, showing the effects of a strong localized vertical transport injecting water vapor into high altitudes. We show the interannual variability of this feature and provide an estimation of the hydrogen escape to space associated to it. The main conclusions are summarized in Section 4.

2 The NOMAD instrument and data analysis

The Nadir and Occultation for MArs Discovery (NOMAD) is an infrared spectrometer covering the spectral range between 0.2 to 4.3 μm. Its Solar Occultation (SO) channel uses an Echelle grating with an Acousto Optical Tunable Filter (AOTF) to select different diffraction orders to be used during the observations. The spectral resolution of the SO channel is $\lambda/\Delta\lambda$=17000, with a vertical sampling of about 1 km. Also, the AOTF permits probing the atmosphere at a given altitude through 6 different diffraction orders [4]. In addition to the water vapor [3], [5], our processing pipeline has been optimized to retrieve temperature [6], carbon monoxide [7] and aerosol [8] vertical profiles, providing a wide overview of the Martian atmosphere.
For this study, we used Level 1 SO calibrated transmittances [9], [10] of diffraction orders 134 (3011 - 3035 cm^{-1}), 136 (3056 - 3081 cm^{-1}) for the lower atmosphere below 60 km, and 168 (3775 - 3806 cm^{-1}), 169 (3798 - 3828 cm^{-1}) for the upper atmosphere above 60 km. We have developed preprocessing tools to identify and eliminate residual artifacts in the spectra (bending, spectral shift) using the line-by-line radiative transfer algorithm KOPRA [11]. During the inversions, we implemented into our Forward Model the latest calibration of the NOMAD AOTF and its instrumental lineshape (ILS) [12]. The retrievals were done combining the spectra of low altitude orders (134,136) with spectra of high altitude orders (168,169) up to 120 km for occultations where those orders were observed simultaneously. For optimization purposes, we only fit the data at certain spectral windows where the strongest H_2O absorption lines are located. The best fit obtained during the inversion is good, with overall vertical resolution of 2-10 km.

3 Results and discussion

We selected observations during and after the perihelion season, covering three similar L_S ranges during MYs 34, 35 and 36: L_S^1=240°-260°, L_S^2=260°-280°, L_S^3=280°-300°. The latitudinal distribution of H_2O is presented in Figure 1. We have binned the retrieved profiles in 5° latitude intervals considering each profile's uncertainty. During these L_S periods, we observed a vertical column of H_2O (denoted as "plume") with abundance about 50 ppmv at 60°S - 30°S reaching altitudes up to 100 km during L_S^2 in MYs 35 and 36 (Fig. 1B2, 1C2). MY 34 also showed a similar structure but with reduced abundance and with a peak showing up later in the season (Fig. 1A3).

We averaged the retrieved profiles within the solar longitude ranges L_S^1, L_S^2 and L_S^3 for each analyzed MY, excluding observations from latitudes between the equator and 45° in order to capture only vertical profiles representative of the observed plume during each MY. The averaged H_2O profiles for each L_S range in the southern hemisphere are presented in Figure 2 for MYs 34, 35 and 36 (panels A, B and C respectively). The difference in ppmv between L_S^2 and L_S^3 profiles is shown in Figure 2D. We observed a clear enhancement of the water abundance above 80 km of about 30 ppmv during L_S^2 in MYs 35 and 36 (orange and green lines), showing a similar vertical structure in both years. In contrast, MY 34 shows an enhancement of only 15 ppm during L_S^3.

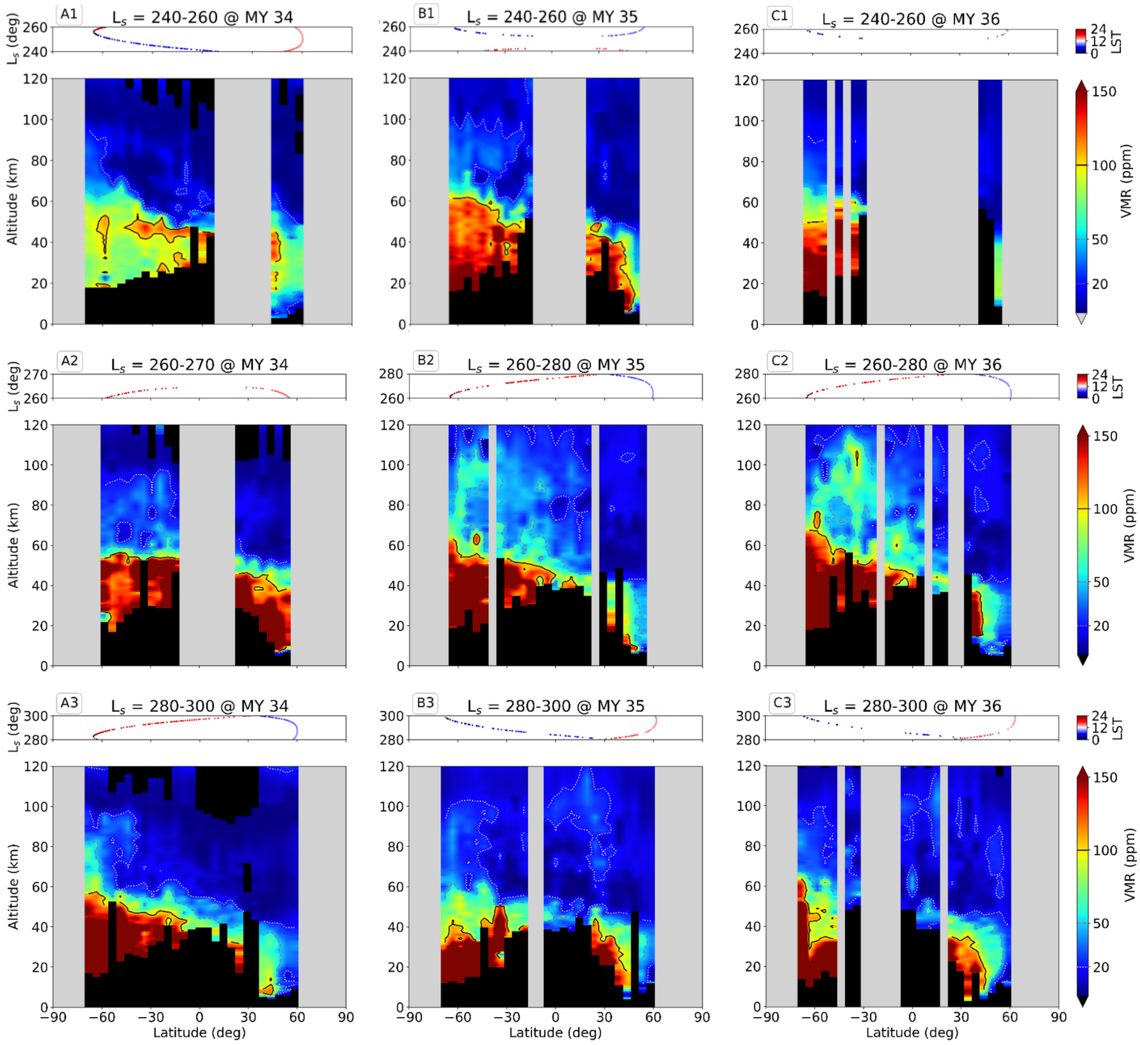

Figure 1: Water vapor latitudinal variation during L_S^1=240°-260° (A1, B1, C1), L_S^2 = 260°-280° (A2, B2, C2) and L_S^3 = 280°-300° (A3, B3, C3) for MYs 34 (left), 35 (middle) and 36 (right). Lines show volume mixing ratio (VMR) contours at 100 (black), 50 (gray) and 20 (white) ppmv. Dots in panels A1-A3, B1-B3, C1-C3 indicate the latitude, Solar Longitude and Local Solar Time of the observations.

We estimated the hydrogen escape flux induced by the observed water vapor plume using a simple photochemical model from [13]. We have averaged all the vertical profiles in the southern hemisphere for latitudes higher than 45°S during the three L_S periods for each MY, as shown in Figure 2. The total contribution to the hydrogen escape for each MY and L_S period is presented in Figure 3. We obtained an integral escape flux associated to the plumes of about $\sim 3.2 \pm 0.5 \times 10^9$ cm^{-2}s^{-1}, which is in a similar range of the hydrogen escape during the perihelion obtained by previous studies [14], [15], [16].

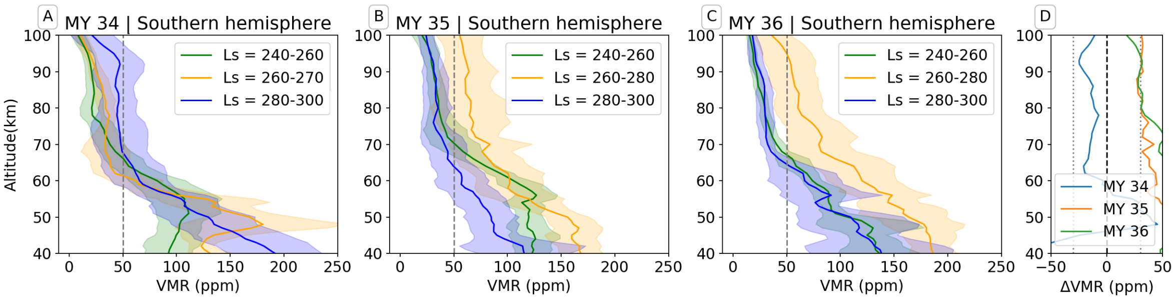

Figure 2: Averaged water vapor volume mixing ratio (VMR) profiles at southern hemisphere during solar longitude ranges L_S^1 = 240°-260° (green), L_S^2 = 260°-280° (yellow) and L_S^3 = 280°-300° (blue) for MYs 34 (A), 35 (B), and 36 (C). Profiles from latitudes below 45° have been excluded in the average. Shaded areas represent the standard deviation of the average. Vertical dashed lines indicate abundance of 50 ppmv. Panel D shows the averaged profiles difference L_S^2 - L_S^3 for MYs 34 (blue), 35 (orange) and 36 (green). Vertical dotted lines indicate abundance differences of ±30 ppmv (dotted) and 0 ppmv (dashed) for reference.

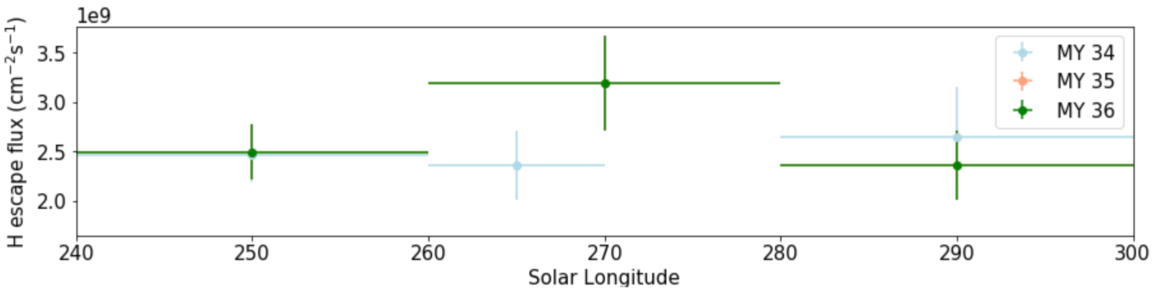

Figure 3: Estimated hydrogen flux for MYs 34 (light blue), 35 (orange) and 36 (green). Note that orange and green points are overlapped.

4 Conclusions

This study focuses on the vertical distribution of water vapor during perihelion and southern summer solstice. We have obtained ∼1000 H_2O profiles from the lower troposphere up to 120 km altitude, with a vertical resolution of 2-10 km. The latitudinal variations over 3 MYs reveal the presence of water vapor in significant amounts in the upper mesosphere, as it is transported vertically at 60°S - 50°S. The main conclusions of this study can be summarized as follows:

- This water vapor plume occurs for a short period (20° in L_S) but repeats during three Martian years (MYs), with a clear interannual variability.
- During non-global dust storm years (MYs 35 and 36), the water vapor injection occurs at L_S = 260° - 280°. During MY 34, the observed plume appears later, with lower abundances above 80 km.

- We attribute this difference to TGO spacecraft sampling variations and to long-term effects of the MY 34 Global Dust Storm, leading to a possible weakening of the Southern Polar Vortex [17] during the storm, enhancing dust deposition over water ice reservoirs and preventing water ice sublimation later in the season [18].
- We provide a rough estimation of the hydrogen escape flux associated to the strong plumes in MYs 35 and 36 of about $\sim 3.2 \pm 0.5 \times 10^9$ cm^{-2}s^{-1} associated to the plumes, which adds to the importance of the perihelion season to the global budget of hydrogen escape on Mars.

Acknowledgments

The IAA/CSIC team acknowledges financial support from the Severo Ochoa grant CEX2021-001131S and by grants PID2022-137579NB-I00, RTI2018-100920J-I00 and PID2022-141216NB-I00 all funded by MCIN/AEI/10.13039/501100011033. A. Brines acknowledges financial support from the grant PRE2019-088355 funded by MCIN/AEI/10.13039/501100011033 and by 'ESF Investing in your future'. ExoMars is a space mission of the European Space Agency (ESA) and Roscosmos. The NOMAD experiment is led by the Royal Belgian Institute for Space Aeronomy (IASB-BIRA), assisted by Co-- PI teams from Spain (IAA-CSIC), Italy (INAF-IAPS), and the United Kingdom (Open University). A.Modak was supported by the Institute for Basic Science (IBSR-035C1).

References

[1] Bibring, J. et al. 2006, Science, 312(5772), 400-404

[2] Montmessin, F. et al. 2017, The atmosphere and climate of Mars, 18, 338

[3] Brines, A. et al. 2024, GRL, 51(14), e2023GL107224

[4] Vandaele, A. C. et al. 2018, Space Science Reviews, 214, 1-47

[5] Brines, A. et al. 2023, JGR: Planets, 128(11), e2022JE007273

[6] Lopez-Valverde, M. A. et al. 2023, JGR: Planets, 128(2), e2022JE007278

[7] Modak, A. et al. 2023, JGR: Planets, 128(3), e2022JE007282

[8] Stolzenbach, A. et al. 2023, JGR: Planets, 128(11), e2022JE007276

[9] Thomas, I. et al. 2022, Planetary and Space Science, 218, 105411

[10] Trompet, L. et al. 2023, Journal of Geophysical Research: Planets, 128(3), e2022JE007279

[11] Stiller, G. et al. 2000

[12] Villanueva, G. et al. 2022, GRL, 49(12), e2022GL098161

[13] Chaffin, M. et al. 2017, Nature geoscience, 10(3), 174-178

[14] Belyaev, D. et al. 2021, GRL, 48(10), e2021GL093411

[15] Bhattacharyya, D. et al. 2017, JGR: Space Physics, 122(11), 11-756

[16] Holmes, J. et al. 2021, Earth and Planetary Science Letters, 571, 117109

[17] Streeter, P. et al. 2021, JGR: Planets, 126(5), e2020JE006774

[18] Gundlach, B. et al. 2011, Icarus, 213(2), 710-719